Double-Site Binding and Anti-/Pro-oxidation of Luteolin on Bovine Serum Albumin Mediated by Copper(II) Coordination

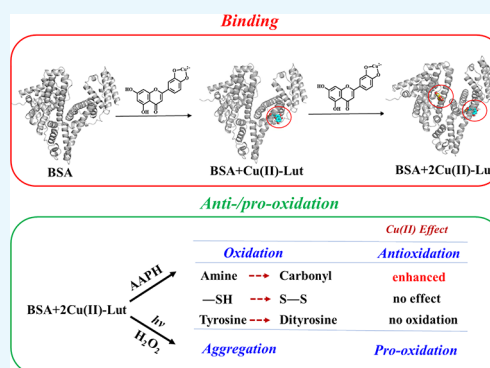Meng-Ting Song, Wen-Zhu Wang, Yao Lu, Rui-Min Han,* Leif H. Skibsted, and Jian-Ping Zhang

ACCESS | Metrics & More | Article Recommendations

ABSTRACT: The interactions of luteolin (Lut) with bovine serum albumin (BSA) mediated by Cu(II) were investigated by spectroscopic, calorimetric, and molecular dynamic (MD) methods. Fluorescence studies showed that the binding of Lut to BSA was significantly enhanced by Cu(II) coordination with the number of binding sites and binding constant increasing from $n = 1$ and $K_a = 3.2 \times 10^5$ L·mol^{-1} for Lut to $n = 2$ and $K_a = 7.1 \times 10^5$ L·mol^{-1} for a 1:1 Cu(II)−luteolin complex, in agreement with the results from isothermal titration calorimetry (ITC). Site-specific experiments with warfarin and ibuprofen and MD confirmed that two binding sites of BSA were sequentially occupied by two Cu(II)−luteolin complexes. Cu(II) coordination increased the antioxidant activity of luteolin by 60% in the inhibition of carbonyl formation from the oxidation of amino groups in the side chain of BSA induced by the peroxyl radical ROO$^\bullet$; however, it counteracted the antioxidant effects of luteolin and played pro-oxidative roles in BSA aggregation induced by $^\bullet$OH.

Binding

BSA | BSA+Cu(II)-Lut | BSA+2Cu(II)-Lut

Anti-/pro-oxidation

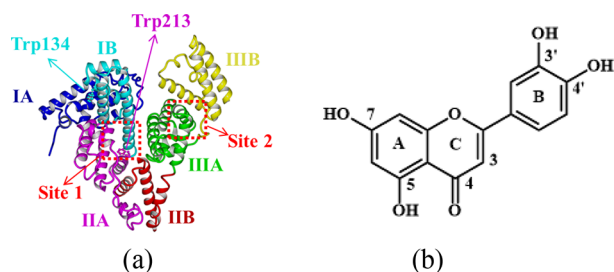|		Cu(II) Effect
Oxidation		*Antioxidation*
Amine	Carbonyl	enhanced
—SH	S—S	no effect
Tyrosine	Dityrosine	no oxidation
Aggregation		*Pro-oxidation*

BSA+2Cu(II)-Lut AAPH / $h\nu$ / H_2O_2

1. INTRODUCTION

Serum albumin (SA) is the most abundant soluble transport protein in the circulatory system of all vertebrates, having many physiological functions such as maintaining the osmotic pressure and pH of blood, and acts as a carrier for the transport of a large number of endogenous and exogenous compounds.[1] Bovine serum albumin (BSA, Scheme 1a) is a main component of whey proteins of milk and commonly used to replace human serum albumin (HSA) to conduct bio-analytical and biochemical studies because of the easy availability, high

Scheme 1. Crystal and Molecular Structure[a]

(a) (b)

[a](a) The crystal structure of bovine serum albumin (BSA) (PDB ID: 4F5S) contains three α-helix domains (I, II, and III), each of which is divided into two subdomains: A and B. The positions of two tryptophan residues (Trp134 and Trp213) and binding sites 1 and 2 for aromatic and heterocyclic ligand are shown. (b) Molecular structure of luteolin (Lut).

stability, ability to bind various ligands, and high structural homology of 76% resemblance with HSA in sequence and conformation.[2] BSA containing 582 amino acid residues is a heart-shaped single polypeptide molecule composed of three structurally homologous α-helix domains (I, II, and III), each of which is divided into two subdomains, A and B, with the structure shown in Scheme 1a.[3] Evolution has developed BSA to bind small biomolecules such as amino acids, fatty acids, flavonoids, and also metal ions.[4−6] Aromatic and heterocyclic ligands as typical for drug molecules generally bind within two hydrophobic pockets of BSA known as site 1 in subdomain IIA and site 2 in IIIA.[3]

Flavonoids are a subclass of polyphenolic compounds that are found in plants, many fruits, vegetables, teas, and wines and have been reported to have potential therapeutic activities for diseases including cardiovascular diseases, cancer, and age-related diseases.[7] The physiological activities of flavonoids are mainly attributed to their antioxidant activities including radical scavenging, metal chelation, as well as enzymatic activity inhibition in forming reactive oxygen species (ROS).[8] A large number of studies including our recent work have

shown that the radical scavenging ability as one of the main indicators of the antioxidant activity of flavonoids is significantly enhanced in a homogeneous ethanol or aqueous model system when the flavonoids are combined with metal ions like Cu(II) and Zn(II) and alkaline earth metal ions including Ca(II), Mg(II), Sr(II), and Ba(II).[9−12]

The interaction between SA and bioactive molecules is of great significance for understanding their transport, absorption, metabolism, and bioavailability.[13] It has been established that the strong binding of different flavonoids to serum albumin (BSA and HSA) with binding constants varying from 10^3 to 10^8 depends on the hydrogen bond, hydrophobic interaction, electrostatic attraction, or a combination of these factors.[14−17] Conformational flexibility and the number of hydroxyl groups in the B ring of the flavonoid were found to significantly affect the binding affinity between flavonoids and serum albumin. The binding sites of most flavonoids with BSA and HSA are located at site 1 in domain IIA. In addition, for metal ions like Cu(II), Zn(II), and Fe(II, III), as micronutrients, metalloproteins are the main binding forms during their uptake, existence, maintenance, and transportation in the human body.[18] In contrast to flavonoids, metal ions bind to BSA and HSA through coordination and complex formation.[19]

Recently, the presence of metal ions has been found to change the binding of flavonoids to BSA. The presence of Cu(II), Zn(II), and Fe(II, III) thus changed binding constants and binding distances between flavonoids and BSA and even caused conformation changes of BSA. Metal ions effects on the interactions of rutin, luteolin, quercetin, and myricetin with BSA were investigated without considering the complex forms of metal coordination with flavonoids.[20−22] In this study, a model system was designed including BSA, Cu(II), and the antioxidant luteolin (Lut, 3′,4′,5,7-tetrahydroxyflavone, Scheme 1b) selected as one of the most bioactive flavonoids in antioxidant and anti-inflammatory aspects.[23] A 1:1 Cu(II)−luteolin complex formed in an aqueous solution at physiological pH from Cu(II) mono-coordination with the 3′,4′ site of Lut has been characterized in our previous work.[24] The present study is focused on the following: (1) Does the Cu(II)−luteolin complex formed in an aqueous solution bind with BSA in the form of a complex or subsequent dissociation? (2) Does Cu(II) coordination to Lut affect the binding of Lut with BSA? (3) Is the remarkably enhanced antioxidant activity of Lut in the presence of Cu(II) seen in homogeneous aqueous solutions transferred to a system containing BSA and will accordingly provide better antioxidant protection against protein oxidation than Lut?

2. MATERIALS AND METHODS

2.1. Materials and Reagents. Luteolin (Lut, >98%) was from Shanxi Huike Plant Co., Ltd. (Shanxi, China), and bovine serum albumin (BSA, ≥98%) was from Sigma Chemical Company (St. Louis, USA). CuSO$_4$·5H$_2$O (>99%) and NaOH (≥96%) were from Beijing Chemical Plant (Beijing, China). 2,2′-Azobis(2-methylpropionamidine) dihydrochloride (AAPH, 98%) was from Energy Chemical (Anhui, China). Warfarin and ibuprofen (≥98%) were from Aladdin Industrial Co. (Shanghai, China). The 30% H$_2$O$_2$ (9.8 M) aqueous solution (≥99.7%) was from Tianjin Fuchen Chemical Reagent Factory (Tianjin, China). The buffer solution used in the experiments was prepared using 3-(N-morpholino)-propanesulfonic acid (MOPS, ≥99.5%, Sigma-Aldrich, St. Louis, MO, USA). All experiments were performed in a 25

mM MOPS buffer at pH 7.4. NaOH was used to adjust the pH, and 3% (v/v) ethanol (99.9%, Fine Chemical Industry Research Institute, Tianjin, China) was used to increase the solubility of Lut. All experimental sections were repeated three times in parallel to produce error analyses.

2.2. Cu(II) Effects on Interaction of Lut with BSA. *2.2.1. UV Spectra.* All UV−vis absorption spectroscopy experiments to record interactions of BSA, Lut, and Cu(II) were performed on a Cary60 spectrophotometer (Varian, Inc., Palo Alto, CA, USA) using a 1 cm quartz cell. The final concentrations of BSA, Lut, and CuSO$_4$ (abbreviated as Cu(II) for simplicity in the following) were 20 μM.

2.2.2. Fluorescence Spectra. Fluorescence spectra were measured using an FS5 fluorescence spectrophotometer (Edinburgh Instruments, UK) with a quartz cell of 1.0 cm thermoneutral at 25 °C. The fluorescence spectra of all samples were first corrected by subtracting the spectra of the buffer alone and further calibrated to eliminate the inner-fitter effect and self-absorption according to the reported method.[25]

For the fluorescence quenching of BSA by Lut, Cu(II), and the Cu(II)−Lut complex, the concentration of BSA was 1.0 μM, and a series of increasing concentrations of Lut and Cu(II) from 0.5 to 5.0 μM were used. The concentration of the Cu(II)−Lut complex was approximately accepted as equal to the concentration of Cu(II) since Cu(II) almost completely coordinated with Lut in a 1:1 (v/v) ratio, which will be further explained in Section 3.1.1. The excitation wavelength λ_{ex} was 295 nm. The site-specific studies were performed using 3.0 μM warfarin and ibuprofen as the markers of site 1 and site 2, respectively. Warfarin and ibuprofen were separately incubated with 1.0 μM BSA for 1 h followed by the gradual addition of Lut or the Cu(II)−Lut complex. The corresponding binding constants (K_a's) and the number of binding sites (n) were evaluated according to the changes in the intensity of fluorescence spectra of BSA quenched by Lut and the Cu(II)−Lut complex.

For the fluorescence determination of dityrosine formed from the oxidation of tyrosine, the excitation wavelength λ_{ex} was 325 nm.

2.2.3. Isothermal Titration Calorimetry (ITC). ITC was used to determine the thermodynamic parameters of the molecular interaction following the method described by Keswani and Kishore.[26] Experiments were carried out on an ultrasensitive microcalorimeter (Microcal ITC200, Malvern Instruments, UK). The final concentrations of BSA, Lut, and the Cu(II)−Lut complex were 20, 300, and 300 μM, respectively. All samples were centrifuged for 10 min before use to remove any precipitates. The BSA solution was placed in a settled sample pool. Lut and the Cu(II)−Lut complex solution were transferred into a syringe and titrated at 25 °C. The MOPS buffer solution containing 3% ethanol was used in the reference tank. The titration data were analyzed by using MicroCal PEAQ-ITC Analysis Software to calculate the thermodynamic parameters.

2.2.4. Molecular Dynamics (MD). 2.2.4.1. System Preparation. The crystal structure of BSA was obtained from the Protein Data Bank (https://www.rcsb.org/), bearing the PDB ID: 4F5S. The MD simulation system consisted of a BSA protein molecule placed in the center of 1.0 nm cube water box (X: 98 Å, Y: 98 Å, and Z: 89 Å) and 15 Cu(II)−Lut complexes placed randomly around the periphery of the structure of BSA, which was filled with water and 0.9% NaCl to maintain the charge balance of the simulation system.

2.2.4.2. Simulation Method. The MD simulations were performed in the YASARA software package[27] to optimize the hydrogen bond network for improving the stability of the system. The pH of the environment was set to 7.4, and the protonation status of amino acid residues was automatically obtained. Prior to the MD simulations, the steepest descent method and the simulated annealing method were used to eliminate the too close contact between atoms of the simulation system. The Amber14 force field[28] was used for the simulation of BSA, GAFF2 force field,[29] and AM1BCC charge[30] for the Cu(II)−luteolin complex and TIP3P for water. During the MD simulations, the temperature was set to 25 °C, and pressure was set to the normal atmosphere. Long distance interaction was calculated using the PME method[31] with a cutoff distance 10 Å. A 1.25 fs step size was used for bonding interactions; and a 2.5 fs step size, for nonbonding interactions.

2.2.5. Docking of Lut and Cu(II) Binding with BSA. Site 1 in subdomain IIA for Lut according to the results in site-specific experiments and the literature[17,32] and the Asp-Thr-His triad in the N-terminal for Cu(II),[33] the two binding sites in BSA, were set as the molecular docking center for Lut and Cu(II), respectively, by using the Autodock 4.2.6 software package.[28] The same crystal structure of BSA as in MD was given as a receptor for molecular docking. The structures of Lut and Cu(II) as donors were geometry-optimized to obtain the PM3[34] atomic charges by the use of MOPAC.[35] Autodock Tools 1.5.6[36] was used to process the structures of BSA, Lut, and Cu(II), respectively, to obtain the pdbqt file. The coordinates of the center of the box docking by Lut and Cu(II) were set as X: 5.92 Å, Y: 23.93 Å, and Z: 106.85 Å, and the box dimension was 126 × 126 × 126 cubic points with a grid point spacing of 0.38 Å. A search space was defined surrounding site 1 for Lut in subdomain IIA of BSA. The number of molecular docking was set to 100, and the remaining parameters were set to default values. The interaction diagrams of Lut and Cu(II) with BSA were generated in PyMOL 1.8.

2.2.6. Circular Dichroism (CD) Spectra. Circular dichroism (CD, Chirascan V100, Applied Photophysics, UK) spectroscopy was used to determine the changes at 180−260 nm in the secondary structures of BSA following the method described by Precupas et al.[37] The concentration for BSA was 3.0 μM, and varying concentrations of 15, 30, and 45 μM were used for Lut, Cu(II), and the Cu(II)−Lut complex. The spectra of all samples were corrected by subtracting the spectra of the blank buffer. The secondary structure contents of BSA were determined using the circular dichroism neutral network (CDNN) software.

2.3. Oxidation and Antioxidation Evaluation. Two methods were used to evaluate the Cu(II) effects on the antioxidation of Lut with BSA: (1) quantitative analysis of the oxidation products of amino acid groups in the side chain of BSA on a micro and invisible level induced by ROO$^{\bullet}$ formed by the pyrolysis of AAPH and (2) kinetic studies of the aggregation of BSA on a macro and visible level induced by an aggressive ROS, $^{\bullet}$OH, produced from the photolysis of H$_2$O$_2$.

2.3.1. Oxidation Product Analysis. The contents of carbonyl and dityrosine groups from the oxidation of amino and tyrosine groups, respectively, and the loss of free sulfhydryl groups were quantitatively determined. The final concentrations of Lut, Cu(II), and Cu(II)−Lut were all 100 μM, and their effects on the oxidation of these amino acid groups in the

side chain were compared in parallel. The sample with BSA alone was used as an example in the following to explain the evaluation method for the oxidation of amino acid groups. The pyrolysis of AAPH was carried out at 37 °C, and the spectroscopic determination for the oxidation products was at 25 °C.

2.3.1.1. Formation of the Carbonyl Group from the Oxidation of Amino Groups. The carbonyl content in oxidized BSA was determined using a protein carbonyl content detection kit (Solarbio, Beijing China) as described by Levine et al.[38] A sample of 112 μM BSA was incubated initially with 25 mM AAPH for 5 h and then derivated with 2,4-dinitrophenylhydrazine (DNPH) for 60 min. The absorbance at 370 nm for the final dinitrophenylhydrazone derivate was measured, and the carbonyl content was calculated according to the method established by Baron et al.[39] and the recommendations by the manufacturer. Carbonyl groups in both Lut and Cu(II)−Lut showed no activity in the reaction with DNPH (*data not shown*), so their interference with the study system can be ruled out. The contents of the carbonyl group for the oxidation of BSA in the presence of Lut, Cu(II), and the Cu(II)−Lut complex were corrected by subtracting the absorbance of Lut, Cu(II), and the Cu(II)−Lut complex, respectively.

2.3.1.2. Formation of Dityrosine from the Oxidation of Tyrosine. A sample of 250 μM BSA was similarly oxidized by the pyrolysis of 25 mM AAPH for 3 h. The content of dityrosine was measured by the fluorescence method under excitation at 325 nm and emission at 420 nm according to the method established by Davies et al.[40]

2.3.1.3. Oxidation and Loss of Sulfhydryls. The sulfhydryl content in BSA was determined using a total sulfhydryl content detection kit (Solarbio, Beijing China) according to Ellman's method described by Di Simplicio et al.[41] A sample of 480 μM BSA was oxidized by the pyrolysis of 100 mM AAPH for 6 h, which further reacted with 3,3′-dithio-bis(6-nitrobenzoic acid) (DTNB). The concentration of sulfhydryl was calculated by measuring the absorbance at 412 nm of the final products using a standard curve obtained with glutathione according to the method described by Chen et al.[42] and the recommendations from the manufacturer.

2.3.2. Photoinduced Oxidation and Aggregation of BSA. The photo-oxidation of 30 μM BSA was initiated by the photolysis of H$_2$O$_2$ to form hydroxyl radicals $^{\bullet}$OH under UV irradiation using a three-black-box analyzer (ZF-7, Beijing Junlibo Biological Technology Co., Ltd., Beijing). The final concentration of H$_2$O$_2$ in all samples was 4.9 μM. The changes in particle size distribution of each sample arising from the photo-oxidation of BSA were measured on a Nano-ZS90 Zetasizer Series (Malvern Instruments, Worcestershire, UK), and the changes in aggregation extents of BSA after 1.0, 1.5 and 2.0 h irradiation were also documented by photographs using a camera. The final concentrations of Lut, Cu(II), and the Cu(II)−Lut complex were all 30 μM, and their effects on the changes in size and aggregation of BSA were also investigated in parallel.

3. RESULTS AND DISCUSSION

3.1. Cu(II) Coordination Effects on the Interaction of BSA with Lut. *3.1.1. Formation of the BSA−Cu(II)−Lut Complex.* Figure 1a shows two characteristic peaks at 268 and 355 nm for Lut, which are attributed to the $\pi \rightarrow \pi^*$ transition of the A ring and B ring.[43] The addition of BSA results in a
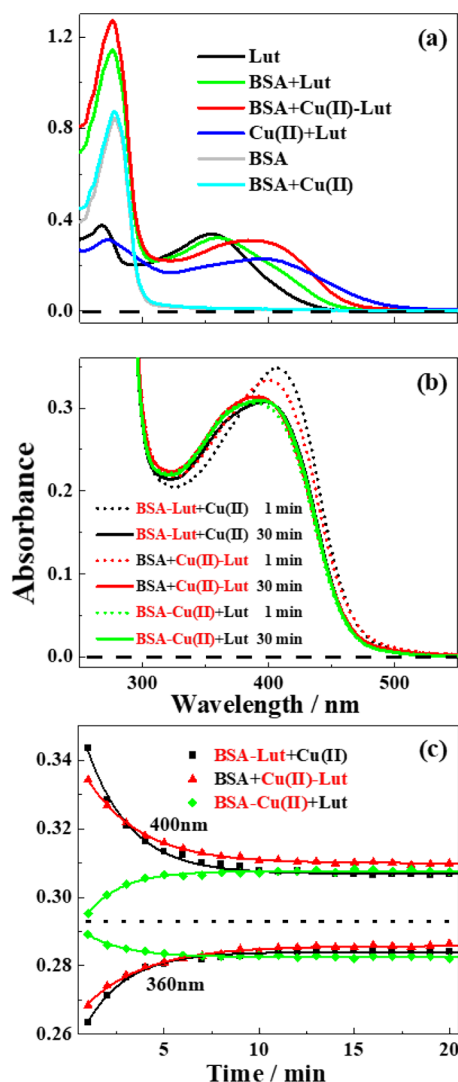
Figure 1. (a) Absorption spectra of Lut, BSA + Lut, BSA + Cu(II)−Lut, Cu(II) + Lut, BSA alone, and BSA + Cu(II). (b) Absorption spectra after 1 and 30 min and (c) corresponding kinetics measured as absorbance at 360 and 400 nm up to 20 min after the addition of Cu(II) to the BSA−Lut complex, addition of the Cu(II)−Lut complex to BSA, and addition of Lut to the BSA−Cu(II) complex. The solid lines were from a single exponential fitting. The concentrations of all solutions including Lut, BSA, and Cu(II) were 20 μM in the 25 mM MOPS buffer aqueous solution at pH ∼ 7.4.

slight absorption decrease in intensity and ∼4 nm red-shift in the lowest absorption band of Lut arising from the increased conjugation in the benzene ring in Lut by the interaction with the amino acid residues in BSA.[44]

A 1:1 Cu(II)−Lut complex has been characterized in our previous work as formed from Cu(II) addition to Lut with a yield of ∼90% by Cu(II) coordination to the 3′,4′-catechol group at a pH ∼ 7.4 aqueous solution with the structure as seen in Scheme 2a, which agreed with the results of Malacaria et al.[45] The 2:1 Cu(II)−Lut complex begins to transform into a 1:1 complex at pH 5.0, which is dominant with a percentage higher than 75% at pH higher than 5.5. The stoichiometry of Lut and Cu(II) complexes obtained by Říha et al.[46] was between 1:1 and 1:2 by determination of ER_{50} values (the concentration ratio of flavonoids to copper when 50% copper is chelated). The difference in stoichiometry between this work

Scheme 2. Protonation of 7-Phenolate for (a) Cu(II)−(Lut−H⁷) in an Aqueous Solution Forming 7-Phenol and for (b) Cu(II)−Lut in a Hydrophobic Environment by Binding with BSA
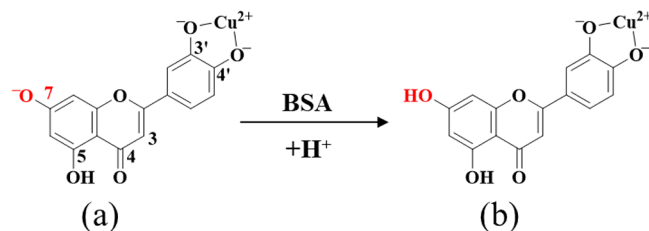
and the present study may arise from the different experimental method used.

The 7-phenol in the Cu(II)−luteolin complex was deprotonated due to the increased acidity followed by Cu(II) coordination at the 3′,4′-catechol group of Lut evidenced by mechanical calculations of the deprotonation enthalpy of each phenolic group.[24]

In the present study, the lowest absorption band of the solution of Cu(II) and Lut addition to BSA showed a +slight blue-shift to the shorter wavelength compared with the spectra of the Cu(II)−Lut complex formed in the absence of BSA. However, the spectral characteristic was different from the complex of Lut alone binding with BSA as seen in Figure 1a, excluding the possibility of Cu(II)−Lut complex dissociation into parent Lut and Cu(II). The new complex formed from the Cu(II)−Lut complex binding with BSA was accordingly ascribed to a 1:1 Cu(II)−Lut complex with 7-phenol protonated due to the hydrophobic environment in BSA as seen in Scheme 2b. As seen in eq 1, the embedding of the protonated Cu(II)−Lut complex to the hydrophobic environment of BSA may promote the formation of the Cu(II)−Lut complex from Cu(II) and Lut in a higher yield close to 100% in the chemical equilibrium of eq 2:

$$Cu(II) - Lut + BSA \rightleftharpoons BSA - Cu(II) - Lut \quad (1)$$

$$Cu(II) + Lut \rightleftharpoons Cu(II) - Lut \quad (2)$$

in which the deprotonation of Lut due to Cu(II) coordination was not shown for clarity. For convenience, Cu(II)−Lut was used to represent the form of 1:1 Cu(II)−Lut complex with 7-phenol protonation after binding with BSA in the following text.

Figure 1b shows the absorption spectra of the solutions by mixing the three samples, BSA, Lut, and Cu(II), following a different addition sequence after 1 and 30 min, including the addition of Cu(II) to the BSA−Lut complex, addition of Cu(II)−Lut to BSA, and addition of Lut to BSA−Cu(II), designated as BSA−Lut + Cu(II), BSA + Cu(II)−Lut, and BSA−Cu(II) + Lut, respectively. It was clearly seen from the similar absorption spectra for both BSA−Lut + Cu(II) and BSA−Cu(II) + Lut to the characteristic absorption spectra of BSA + Cu(II)−Lut, which implied that the same BSA−Cu(II)−Lut complex was formed as the most stable form, no matter the three species, Cu(II), Lut and BSA, initially in any sequence binding together. Cu(II) and Lut bound to BSA as a complex form, not as an individually independent form.

The kinetics was monitored at 360 and 400 nm as shown in Figure 1c for the transformation from the initial reactants to the final and stable BSA−Cu(II)−Lut complex that occurred with a similar first order of rate constants $k = 0.33−0.58$ min^{-1}
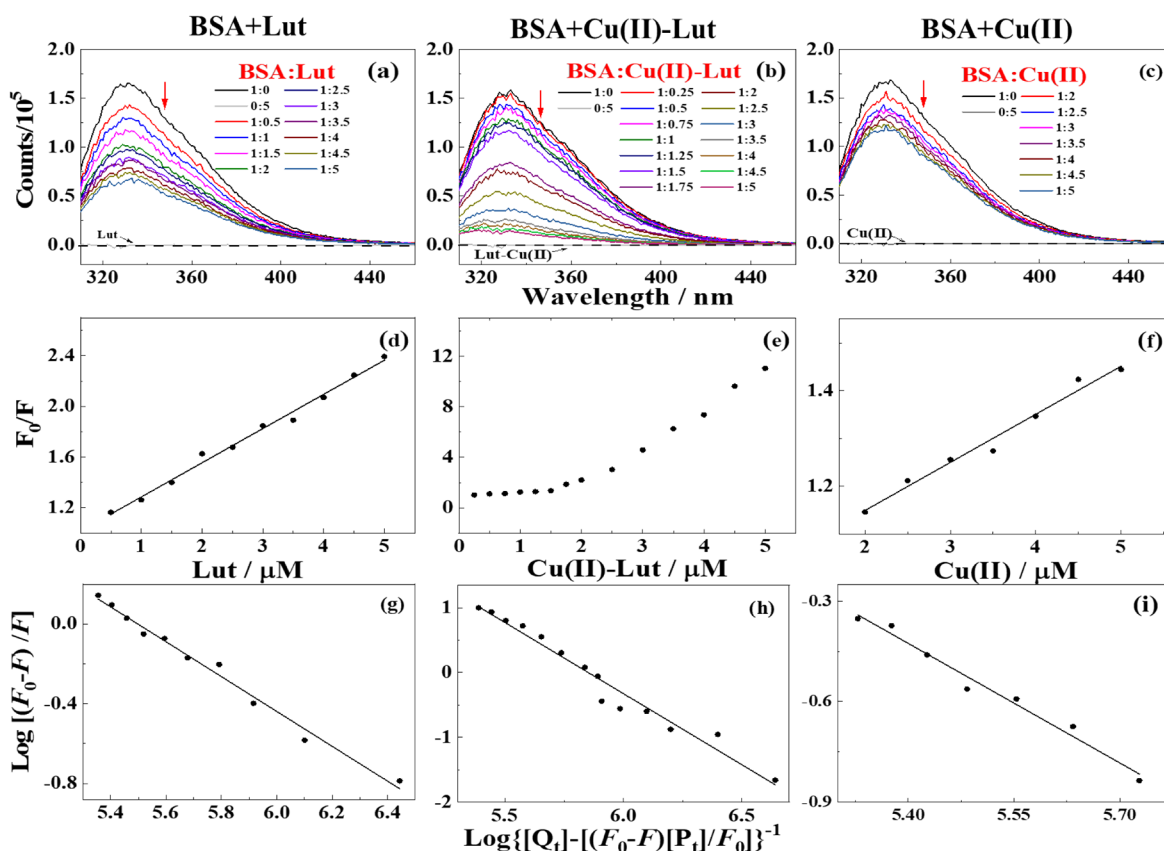
Figure 2. Fluorescence emission spectra of 1.0 μM BSA in the presence of quenchers in varying concentration ratios for (a) Lut, (b) the Cu(II)–Lut complex, and (c) Cu(II) in the 25 mM MOPS buffer aqueous solution at 25 °C. (d, e, f). Stern–Volmer plots and (g, h, i) double-logarithm curves for the data from panels a, b, and c, respectively. λ_{ex} = 295 nm; pH ∼ 7.4; spectral resolution = 2 nm. F_0 and F are the fluorescence intensities of BSA in the absence and presence of quenchers. $[Q_t]$ and $[P_t]$ are the concentrations of the quenching agent and BSA, respectively. The fluorescence emission of individual Lut, the Cu(II)–Lut complex, and Cu(II) is also shown in panels a–c for comparison.

as obtained by single exponential fitting. The BSA–Cu(II)–Lut complex reached a stable form at ∼10 min. The following experiments all started from the addition of Cu(II)–Lut to BSA, and the samples were incubated for ∼10 min prior to experiments.

3.1.2. Fluorescence Quenching. The chromophores of fluorescence in BSA arise from two tryptophan residues with intrinsic fluorescence, one in position 134 (located on the surface) and the other one in position 213 (located within a hydrophobic pocket of protein)[47] as seen in Scheme 1a. The dominant fluorophore is the indole group of tryptophan that absorbs at ∼295 nm and emits at ∼340 nm. The fluorescence intensity of tryptophan may be changed by any accessible quenchers.

Figure 2a,b shows the calibrated fluorescence emission spectra of BSA appearing at 333 nm as the maximum peak with λ_{ex} = 295 nm excitation in the presence of Lut and Cu(II)–Lut. The intensity of fluorescence spectra decreased with the increasing addition of both Lut and Cu(II)–Lut, but the coordination of Cu(II) to Lut showed a more remarkable decrease in the intensity of fluorescence than Lut alone. Lut or Cu(II)–Lut alone showed little if any fluorescence under the same conditions. The fluorescence spectra of BSA by the addition of Cu(II) alone were also recorded for comparison (Figure 2c), showing less effect on the decrease in fluorescence intensity.

When considering the effect of individual Lut or Cu(II) on the fluorescence spectra of BSA, there was no shift of the

maximum emission peak as seen in Figure 2a,c. This suggested that the interactions of Lut and Cu(II) with BSA hardly changed the proximal environment of tryptophan residues in chromophore.[48] Meanwhile, the fluorescence spectra of BSA in the presence of Cu(II)–Lut showed two different processes depending on the concentration of Cu(II)-Lut: for 0.25–5.0 μM, similar to Figure 2a,c, no spectral shift was seen; for 0.5–5.0 μM, a significant blue-shift in spectra was seen, indicating that a stronger interaction of Cu(II)–Lut with BSA occurred with increasing addition of Cu(II)–Lut compared to Lut or Cu(II) alone. A similar blue-shift in spectra was also observed for sinapic acid and its Cu(II) complex as well as luteolin and oxidovanadium(IV) complex binding with BSA, observations that were explained by a change in the chromophore of tryptophan, indole, being placed/buried in a more hydrophobic environment.[49,43]

The bimolecular quenching constants of Lut and Cu(II) with BSA K_q = 5.4 × 10^{13} and 2.1 × 10^{13} L·mol^{-1}·s^{-1} were determined by linear regression of the fluorescence intensity ratio (Figure 2d,f) against the concentration of Lut or Cu(II) using the Stern–Volmer equation.[50] The linear relationships implied only a single class of tryptophan fluorophores in the BSA environment equally accessible to quenchers and by a single quenching mechanism, either dynamic or static.[48] Dynamic quenching can be excluded in the present case, and a static process was confirmed for Lut and Cu(II) due to larger quenching constants than the maximum diffusion collision quenching constant of 1.0 × 10^{10} L·mol^{-1}·s^{-1}.[48] However, the

Table 1. The Binding Constants (K_a, L·mol⁻¹), the Number of Binding Sites and Stoichiometry (N), Thermodynamic Parameters' Change in Enthalpy ΔH (kcal/mol), Gibbs Free Energy ΔG (kcal/mol), and Entropy $-T\Delta S$ (kcal/mol) for the Interactions of Lut, Cu(II)−Lut, and Cu(II) with BSA[a]

samples	K_a (×10⁵) (L·mol⁻¹)	n	ΔH (kcal/mol)	ΔG (kcal/mol)	$-T\Delta S$ (kcal/mol)
BSA + Lut	3.2 ± 0.2[1]/1.0 ± 0.2[2]	0.9 ± 0.1[1]/1.3 ± 0.1[2]	−2.51 ± 0.24	−6.86 ± 0.13	−4.33 ± 0.36
BSA + Cu(II)−Lut	7.1 ± 0.7[1]/2.0 ± 0.2[2]	2.2 ± 0.1[1]/2.3 ± 0.1[2]	−0.60 ± 0.01	−7.45 ± 0.04	−6.86 ± 0.04
BSA + Cu(II)	1.1 ± 0.4[1]/----	1.2 ± 0.1[1]/----	-----	-----	-----

[a]Superscripts 1 and 2 represent data obtained from the fluorescence quenching of BSA and the ITC curves, respectively. ----, not available.
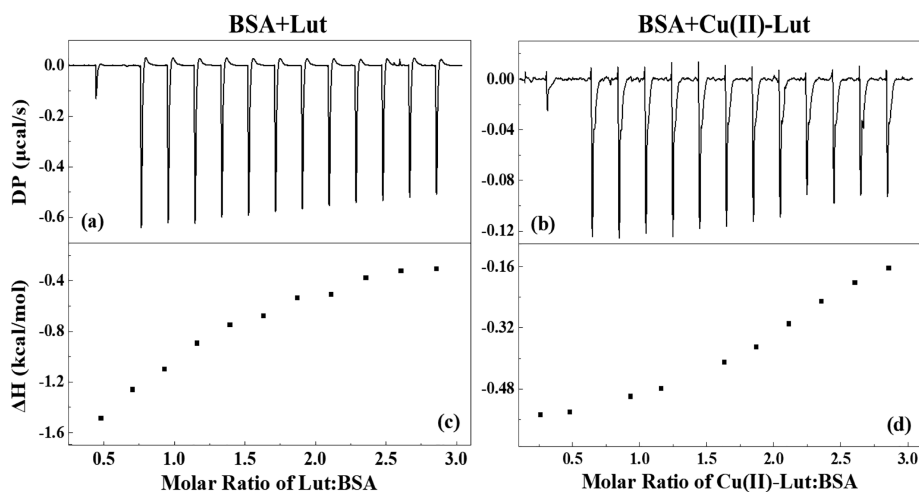

Figure 3. ITC titration thermographs of 20 μM BSA by addition of 300 μM (a, c) Lut and (b, d) Cu(II)−Lut complex. (a, b) Simulated raw injection data and (c, d) integrated injection data in 25 mM MOPS at pH 7.4 and 25 °C. DP (μcal/s) and ΔH (kcal/mol) represent the changes in differential power and heat for each injection against the molar ratio of Lut/Cu(II)−Lut and BSA, respectively.

deviation of the Stern−Volmer plot from linearity (upward curvature) for Cu(II)−Lut suggested that there is more than one class of tryptophan fluorophores in the BSA environment and is explained by a combination of a static and dynamic process.[48]

The binding constants—K_a = 3.2× 10⁵, 7.1 × 10⁵, and 1.1 × 10⁵ L·mol⁻¹—and the number of binding sites—n = 0.9, 2.2, and 1.2—for Lut, Lut−Cu(II), and Cu(II) with BSA, respectively, were calculated by fitting according to the double-logarithm equation[51] as shown in Figure 2g−i, and the results are summarized in Table 1. The results meant that Cu(II) coordination to Lut not only promoted one more Lut molecule further binding with BSA but also elevated the binding constants of Cu(II)−Lut, ~2.2 times of Lut, which was different from Fe(II) coordination to rutin resulting in the decrease in binding constant and keeping mono-site binding with BSA as the parent rutin.[52]

3.1.3. Site-Specific Experiments. A site-specific experiment was performed to further explore the binding sites of Lut and Cu(II)−Lut with BSA. Warfarin and ibuprofen have been extensively reported as site makers of BSA mainly locating at subdomains IIA (site 1) and IIIA (site 2), respectively.[53] The binding constants (K_a) in the presence of 3.0 μM warfarin and ibuprofen were calculated by fitting according to the double-logarithm equation.[51] For the BSA−Lut system, the binding constant decreased from 3.2 × 10⁵ to 1.6 × 10⁵ L·mol⁻¹ by the addition of warfarin, indicating that Lut and warfarin competed for binding at site 1 in BSA. In contrast, the presence of ibuprofen only slightly reduced the binding constant of Lut with BSA to 2.9 × 10⁵ L·mol⁻¹, indicating that Lut almost did not bind at site 2. For the BSA−Cu(II)−Lut system, both warfarin and ibuprofen to some extent reduced the binding

constants of Cu(II)−Lut with BSA from 7.1 × 10⁵ to 6.3 × 10⁵ and to 6.6 × 10⁵ L·mol⁻¹, respectively, confirming that Cu(II)−Lut molecules competed with warfarin and ibuprofen in binding to BSA separately at two different sites in BSA, i.e., sites 1 and 2. The reduction of the binding constants for the BSA−Cu(II)−Lut system was not so obvious as that for the BSA−Lut system, which may arise from the stronger binding of Cu(II)−Lut to BSA than Lut.

3.1.4. Isothermal Titration Calorimetry (ITC). ITC was used to further investigate the binding information including thermodynamic parameters of Lut and Cu(II)−Lut with BSA. Figure 3a,b shows the titration thermograms of BSA titration with 300 μM Lut and 300 μM Cu(II)−Lut, where each peak corresponded to a single injection of the Lut or Cu(II)−Lut solution. The titration curve values were all positive, and the binding was accordingly exothermic for both Lut and Cu(II)−Lut binding with BSA with ΔH < 0.

Figure 3c,d represents the cumulated amount of heat per mole of injectant against the molar ratio of Lut or Cu(II)−Lut and BSA, which demonstrated that saturation occurred at a molar ratio ~ 2.5 during the binding of Lut to BSA, while for Cu(II)−Lut binding to BSA, saturation cannot be seen within the detection range. This observation implied that higher molar ratio values were required for the saturation of Cu(II)−Lut binding to BSA. The experimental data were best accounted for by using a "single-set of binding sites" model giving the following stoichiometry and binding constants with BSA: n = 1.3 and K_a = 1.0 × 10⁵ L·mol⁻¹ for Lut and n = 2.3 and K_a = 2.9 × 10⁵ L·mol⁻¹ for Cu(II)−Lut, respectively. These results further supported the 2 Cu(II)−Lut but 1 Lut molecule binding to BSA and Cu(II) coordination enhancing the strength of Lut binding with BSA. The binding constants
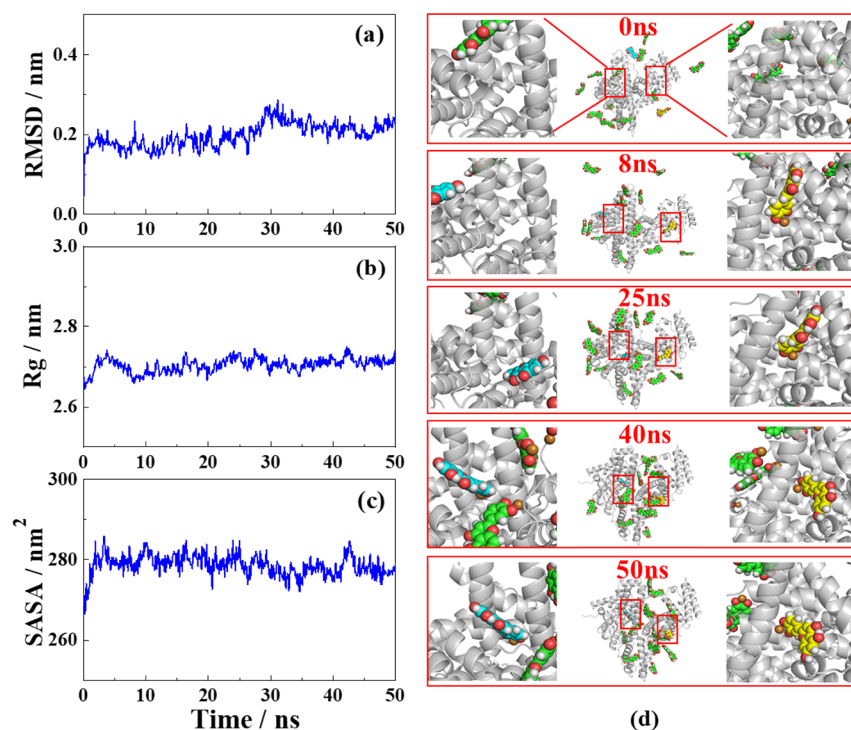
Figure 4. The kinetic changes of BSA in (a) the root mean square deviation (RMSD) values, (b) radius of gyration (Rg), and (c) solvent accessible surface area (SASA) by Cu(II)−Lut complex binding with the simulation time. (d) The binding process of the Cu(II)−Lut complex to site 2 followed by site 1 in BSA at the indicated simulation time.

from ITC were lower than the values from fluorescence quenching, which were also found by Precupas et al.,[37] but the magnitudes of increase for the two methods, 2.9 times for ITC and 2.2 times for fluorescence quenching, were similar.

Thermodynamic parameters for the interactions of Lut and Cu(II)-Lut with BSA, including enthalpy change ΔH, change in Gibbs free energy ΔG, and entropy change $−T\Delta S$, were obtained using the MicroCal PEAQ-ITC Analysis Software and summarized in Table 1. Generally, the interactions between small molecules and biomacromolecules are considered to be a process driven by both enthalpy and entropy. The positive values of entropy variation ΔS in both BSA−Lut and BSA−Cu(II)−Lut systems supported that hydrophobic forces dominated the expulsion of water molecules from the cavity of BSA, transforming into more random configurations, and drove the formation of the BSA−Lut and BSA−Cu(II)−Lut complexes as other BSA−polyphenol systems.[54] The larger entropy variation, −6.86 kcal/mol for Cu(II)−Lut binding to BSA, may be due to two Cu(II)−Lut molecules liberating more water than the system of one Lut molecule binding to BSA with a lower entropy variation, −4.33 kcal/mol.

The enthalpy changes ΔH and free energy changes ΔG were both negative as presented in Table 1, indicating that the two systems were both exothermic and spontaneous binding processes. The negative value of ΔH (−0.60 kcal/mol) for the BSA−Cu(II)−Lut system containing charged Cu(II) was very small and close to zero. This implied that electrostatic interaction occurred together with hydrophobic interaction to drive Cu(II)−Lut binding to BSA. In contrast, the negative ΔH value (−2.51 kcal/mol) for the BSA−Lut system was more negative, supporting that hydrogen bonding interaction also occurred during Lut binding to the amino acid groups of BSA for Lut with two more phenol groups than Cu(II)−Lut.

However, both fluorescence quenching and ITC results cannot support the sequential binding model due to the coexistence of different complexation states in mutual equilibrium and cannot confirm any binding order or mechanism.[37]

3.1.5. Molecular Dynamics (MD) Simulations and Docking. Computational-based molecular modeling techniques, MD simulations, were applied to investigate the stability and dynamics of Cu(II)−Lut binding to BSA and the conformational binding mode of the BSA−Cu(II)−Lut complex.

The stability of the BSA−Cu(II)−Lut system was tested by analyzing the root mean square deviation (RMSD) values of the skeleton atoms in BSA as seen in Figure 4a. The result indicated that the system tends to be stable within a 50 ns timescale with a lower value of RMSD = 0.198 ± 0.030 nm. Similarly, the variations of the radius of gyration (Rg) in Figure 4b and the solvent accessible surface area (SASA) in Figure 4c were both also stable during the simulation time. These results supported that the MD calculations on the BSA−Cu(II)−Lut system were reliable.

To explore the dynamics or the sequence of the free Cu(II)−Lut binding to the cavity of BSA, the representative conformations within the 50 ns simulation process were visualized, and the results are shown in Figure 4d. In the initial state, 15 Cu(II)−Lut molecules were located in the solution environment outside BSA as seen for conformation at 0 ns. At 8 ns, a Cu(II)−Lut molecule actively began to be close to/ located at the surface of the active pocket of site 2 in the cavity of BSA, while site 1 did not yet bind any Cu(II)−Lut molecules at this time. At 25 ns, the binding of Cu(II)−Lut with site 2 went deeper into the pocket, and meanwhile, a second Cu(II)−Lut began to approach the surface of site 1. Up to 40 ns, the first Cu(II)−Lut at site 2 had been stable enough,
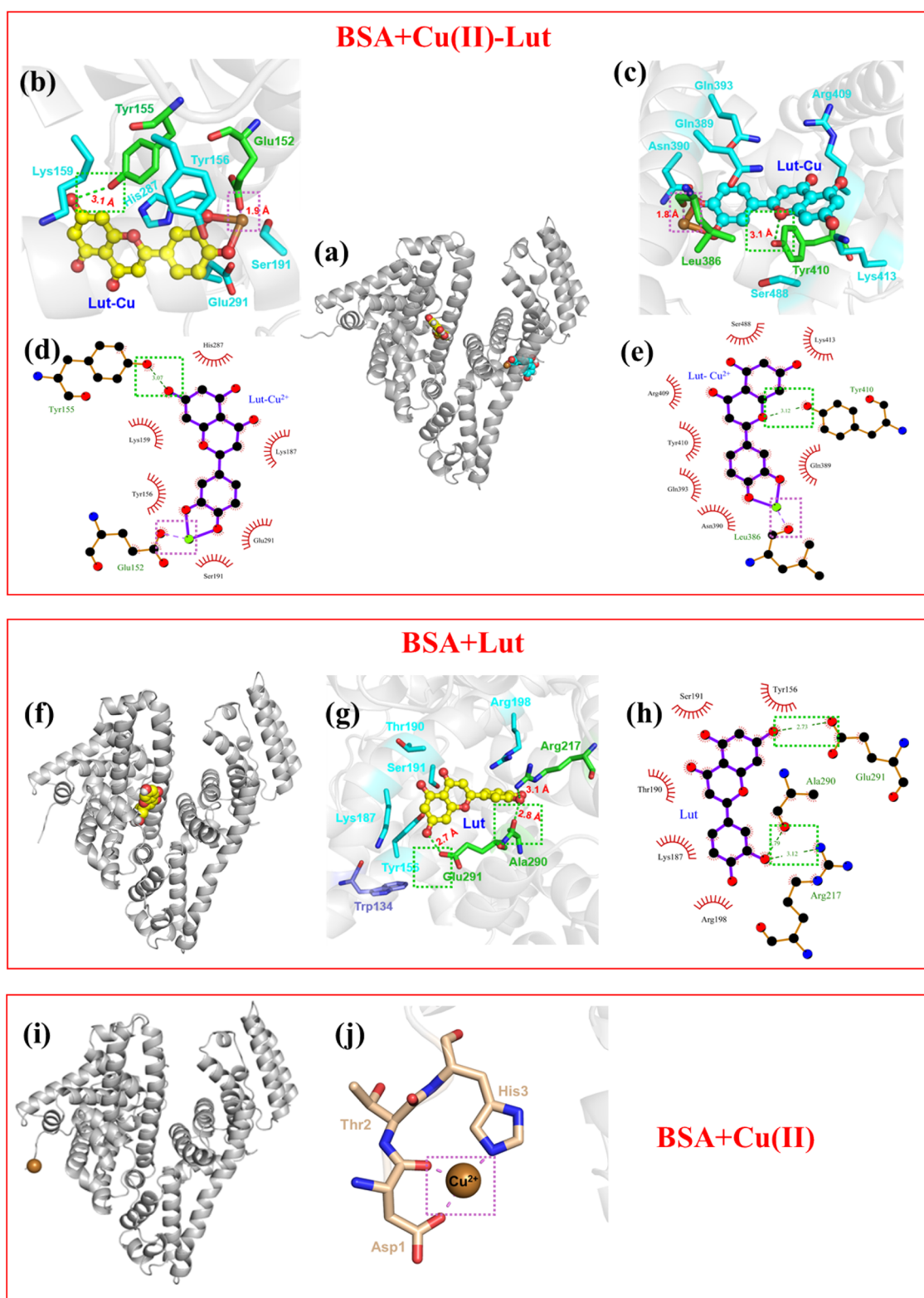
Figure 5. (a, f, i) Integral and localized (b, c, g, j) three- and (d, e, h) two-dimensional diagrams for the binding patterns of the Cu(II)−Lut complex (upper), Lut (intermediate), and Cu(II) (lower) to BSA, respectively. In two-dimensional diagrams (d, e, h), the red gears represent hydrophobic interaction, the green dotted lines represent hydrogen bonding, and the dotted purple lines represent electrostatic interaction. For the complex of BSA + Cu(II), only three- and not two-dimensional diagrams are shown due to the simpler binding pattern.

and the second Cu(II)−Lut close to site 1 began to bind into the pocket of the cavity. Until 50 ns, two Cu(II)−Lut complexes bound to the pockets at both site 2 and site 1 in Figure 4d.

The above analysis showed that Cu(II)−Lut could spontaneously bind to site 2 followed by binding to site 1 in BSA from the solution environment forming a stable BSA−Cu(II)−Lut complex with the conformation as seen in Figure

5a. The detailed binding patterns of Cu(II)−Lut at site 1 and site 2 were enlarged and are shown in Figure 5b−e. For the two Cu(II)−Lut molecules binding at site 1 (*left*) and site 2 (*right*) in the three-dimensional (Figure 5b,c) and two-dimensional (Figure 5d,e) diagrams, the analyses on the interaction forces showed that the hydrophobic interactions between the aromatic rings of Lut as a ligand in both Cu(II)−Lut molecules and amino acid groups surrounding were the dominant interaction force to stabilize Cu(II)−Lut binding to the pocket. Meanwhile, electrostatic interactions between Cu(II) in two Cu(II)−Lut molecules and the oxygen atom of the amino acid were found, further enhancing the affinity between Cu(II)−Lut and BSA. They were in good agreement with the results obtained from ITC that hydrophobic interaction and electrostatic interaction jointly drove Cu-(II)−Lut binding to BSA. In addition, a hydrogen bond interaction between the amino acid group and Lut in Cu(II)−Lut at both site 1 and site 2 was also helpful as a minor force to drive Cu(II)−Lut binding to BSA. In contrast, more hydrophobic groups were found for Cu(II)−Lut in site 2 than in site 1, which may produce a stronger driving force to induce Cu(II)−Lut preferentially binding to site 2 of BSA followed by site 1.

Docking simulations on individual Lut and Cu(II) were also performed for comparison with Cu(II)−Lut. The three- and two-dimensional binding patterns of Lut with BSA at site 1 are shown in Figure 5f−h. Lut mainly bound to the cavity composed of Tyr156, Lys187, Thr190, Ser191, Arg198, Arg217, Ala290, and Glu291. Hydrophobic interactions of the aromatic ring of Lut with amino acids surrounding (Tyr156, Lys187, Thr190, Ser191, and Arg198) were the dominant interaction force, and the hydrogen bonds with Arg217, Ala290, and Glu291 further enhanced the affinity between Lut and BSA. The results were consistent with the thermodynamics parameters from ITC. In contrast, Cu(II) bound with BSA at the Asp-Thr-His triad in the N-terminal. The binding positions of Cu(II) with BSA shown in Figure 5i,j indicated that Cu(II) coordinated to two oxygen atoms and one N atom of amino acids. The establishment of a coordination bond was thus concluded to be an important driving force of molecular recognition between Cu(II) and BSA.

Compared with Lut, a larger hydrophobic area of both two Cu(II)−Lut molecules at site 1 and site 2 with BSA may promote the double-site binding and increase the binding strength of Cu(II)−Lut with BSA. Electrostatic interactions of Cu(II)−Lut with BSA, absent an interaction of Lut with BSA, may further enhance these effects for the Cu(II)−Lut complex.

3.1.6. CD Spectra. CD spectra were recorded to provide information of the changes in the secondary structure including the α-helix, β-sheet, and random coil by the addition of Lut, Cu(II)−Lut, and also Cu(II) for comparison as shown in Figure 6a−c. The negative peaks of BSA alone at 208 and 222 nm in Figure 6a were both contributed by n−π* transition of the peptide bond in α-helix.[55] With increasing addition of Lut, Cu(II)−Lut, and Cu(II), the intensity of the characteristic peak of BSA α-helix decreased gradually with no obvious shift of the maximum wavelength, and the reduction amplitude positively correlated with the concentration. The specific contents of the secondary structure of BSA are listed in Table 2, indicating the increase in β-sheet, β-turn, and random coil accompanying the decrease in α-helix. This suggested that Lut, Cu(II)−Lut, and Cu(II) all can unfold the α-helix structure of
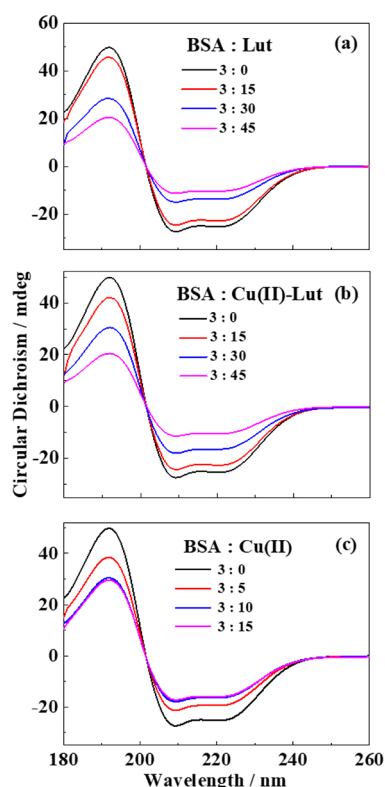

Figure 6. CD spectra of 3.0 μM BSA by the addition of varying concentrations of (a) Lut, (b) the Cu(II)−Lut complex, and (c) Cu(II) as indicated.

BSA with transformation into other forms of secondary structures. In contrast, the reduction in the intensity of CD signals caused by Lut was most significant among the three samples followed by Cu(II) and Cu(II)−Lut. Compared with Lut, the content of α-helix in BSA by binding with Cu(II)−Lut was ∼40% higher than that by binding with Lut at both concentrations of 30 and 45 μM, implying that Cu(II) coordination to Lut was more favorable in improving the stability of α-helix in BSA. The double-site binding of two Cu(II)−Lut molecules probably balanced the effects of each mono-site binding on the α-helix structure, resulting in a more stable secondary structure.

3.2. Cu(II) Effects on the Oxidation and Antioxidation of BSA by Coordination with Lut. *3.2.1. Oxidation Product Analysis Initiated by the Pyrolysis of AAPH. 3.2.1.1. Oxidation of Amine and Formation of the Carbonyl Group.* Figure 7a depicts the formation of carbonyl compounds during the oxidation of the amino group in the absence and presence of Lut, Cu(II)−Lut, and Cu(II) after incubating with the initiator AAPH for 5 h at 37 °C. Compared with BSA alone, the addition of Lut and Cu(II)−Lut both reduced the generation of carbonyl compounds and showed clear antioxidant effects. Cu(II) coordination to Lut showed remarkably synergistic antioxidation activities, and the joint effects of Cu(II) and Lut on the inhibition efficiency of the oxidation of amino groups were ∼60% higher than the effect of Lut alone. In contrast, Cu(II) itself showed an obvious pro-oxidation effect on BSA, approximately 14% higher than the sample with BSA alone.

It can be seen from Scheme 3a that there was a large amount of amino acid residues with free amino groups, such as arginine, asparagine, glutamide, and lysine, which distributed

Table 2. Effects of Lut, the Cu(II)−Lut Complex, and Cu(II) at Indicated Varying Concentrations on the Secondary Structures of 3.0 μM BSA

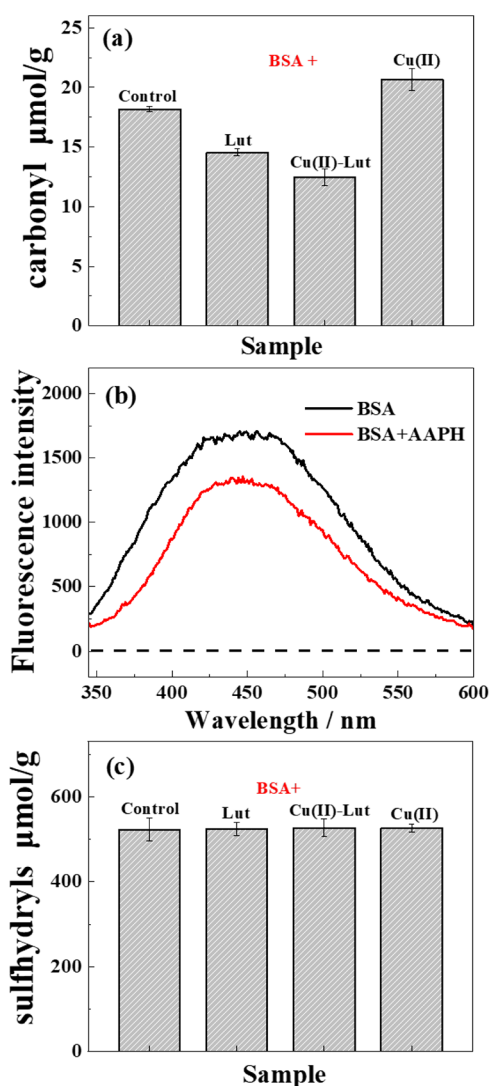| samples	Lut/Cu(II) (μM/μM)	α-helix (%)	β-sheet (%)	β-turn (%)	random coil (%)
BSA	0:0	50.3 ± 0.9	9.9 ± 0.5	12.7 ± 0.9	33.3 ± 2.3
BSA + Lut	15:0	45.5 ± 0.6	11 ± 0.7	13.4 ± 0.8	34.5 ± 2.1
	30:0	31.3 ± 0.3	17.4 ± 1.1	15.6 ± 0.9	37.8 ± 1.9
	45:0	28.1 ± 1.7	20.2 ± 1.3	16 ± 1.4	39.1 ± 2.2
BSA + Cu(II)-Lut	15:15	46.9 ± 2.1	12.1 ± 1.4	13.7 ± 0.9	30.9 ± 1.2
	30:30	46.1 ± 0.7	9.1 ± 0.2	14.8 ± 0.1	24.1 ± 0.1
	45:45	38.8 ± 0.8	12.7 ± 0.3	15.9 ± 0.1	28.7 ± 0.2
BSA + Cu(II)	0:15	39.4 ± 0.3	13 ± 1.4	14.3 ± 0.9	36.2 ± 2.4
	0:30	34.2 ± 0.5	15.6 ± 1.7	15.1 ± 0.7	37.5 ± 1.7
	0:45	32.8 ± 0.4	17.7 ± 0.3	17 ± 0.1	32.4 ± 0.2

Figure 7. (a) The production of carbonyl for BSA alone, BSA + Lut, BSA + Cu(II)−Lut, and BSA + Cu(II) after incubation with 25 mM AAPH for 5 h with [BSA] = 112 μM. (b) Fluorescence emission spectra of BSA and BSA−AAPH after incubation with 25 mM AAPH for 3 h with [BSA] = 250 μM. λ_{ex} = 325 nm. (c) Changes in free sulfhydryl contents of BSA, BSA + Lut, BSA + Cu(II)−Lut, and BSA + Cu(II) after incubation with 100 mM AAPH for 6 h with [BSA] = 480 μM. In both panels (a) and (c), [Lut] = [Cu(II)] = [Cu(II)− Lut] = 100 μM. The incubation temperature of AAPH was 37 °C, and spectral measurements were carried out at 25 °C for all samples in the aqueous MOPS buffer at pH ~ 7.4 in panels (a), (b), and (c).

around site 1 and site 2 for Lut and Cu(II)−Lut binding as well as around the N-terminal of BSA for Cu(II) binding. The obviously increased antioxidation reactivity of Cu(II)−Lut in C=O formation during the oxidation of BSA may arise from the increased radical scavenging reactivity of Lut by Cu(II) coordination as we observed previously in a homogeneous solution.[24] The pro-oxidation effect of Cu(II) was explained as the catalyzed dissociation of hydroperoxide ROOH by Cu(II) to form more oxidizing radicals as in eqs 3 and 4.[56,57]

$$Cu^{2+} + ROOH \rightarrow Cu^{+} + ROO^{\cdot} + H^{+} \qquad (3)$$

$$Cu^{+} + ROOH \rightarrow Cu^{2+} + RO^{\cdot} + OH^{-} \qquad (4)$$

in which ROOH was suggested to form from hydrogen abstraction from BSA by ROO[•] generated from the pyrolysis of AAPH. Cu(II) initially coordinated to BSA at the Asp-Thr-His triad in the N-terminal changed into double-site coordination at two pockets by complexation with Lut, which converted Cu(II) from a pro-oxidant into a protein antioxidant.

3.2.1.2. Oxidation of Tyrosine Forming Dityrosine. Figure 7b shows the fluorescence emission spectra of BSA alone and the solution of BSA + AAPH under excitation at 325 nm at 25 °C after incubation for 3 h at 37 °C. The maximum emission wavelength of BSA appeared at 450 nm. The enhanced fluorescence emission peak of dityrosine with a maximum peak at 420 nm formed from the oxidation of tyrosine has been well-documented,[42] while it was not observed in the present study. On the contrary, the presence of AAPH slightly reduced the fluorescence emission intensity of BSA at 450 nm. This probably arose from having less tyrosine groups than amino groups in BSA and the benzene ring of tyrosine residing inside the more hydrophobic helix structures of BSA (Scheme 3b) limiting the oxidation of tyrosine groups and the formation of dityrosine. It was difficult for tyrosine to compete with the amino groups to get close to ROO[•] initially produced from the pyrolysis of hydrophilic AAPH and to be oxidized. It was also reported by Ignasiak et al.[58] that dityrosine production could not be observed by fluorescence spectroscopic determination during the oxidation of dipeptide containing tyrosine.

3.2.1.3. Oxidation and Loss of Sulfhydryl. Considering every BSA molecule containing only one free sulfhydryl group, a series of concentrations of BSA (30−480 μM) were tried in the determination of the oxidation of sulfhydryl. However, there was no remarkable difference observed for the four investigated samples with the concentration of BSA even up to 480 μM. Figure 7c describes the changes of free sulfhydryl groups in the presence of Lut, Cu(II)−Lut, and Cu(II) after

Scheme 3. Locations of Amino Acids Containing (a) Free Amino Groups, Arginine (Red), Asparagine (Green), Glutamine (Blue), and Lysine (Purple); (b) Tyrosine; and (c) Cysteine in BSA
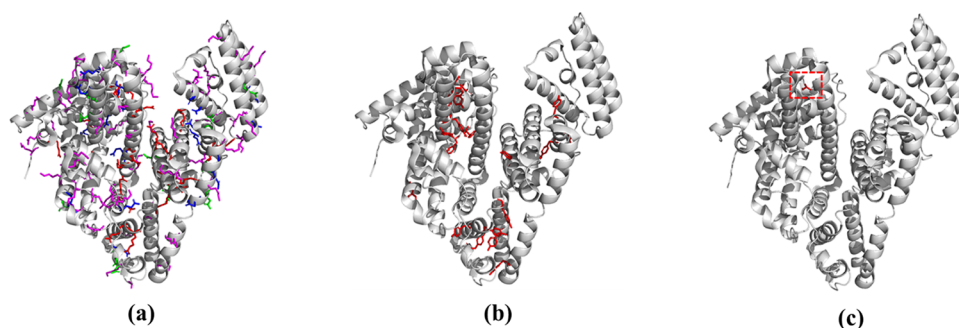
incubating BSA with the initiator AAPH at 37 °C for 6 h. Compared with BSA alone, the addition of Lut, Cu(II)−Lut, and Cu(II) had little effect on the content of free sulfhydryl groups in BSA. This might be accounted for by the presence of only one free sulfhydryl group in BSA as seen in Scheme 3c. The binding sites of Lut, Cu(II)−Lut, and Cu(II) were all not close to this sulfhydryl group, without possibilities for redox interaction.

3.2.2. Photoinduced Oxidative Aggregation of BSA. Compared to ROO•, •OH formed from the photolysis of H_2O_2 is more vigorous, smaller in size, and accordingly more aggressive to oxidize BSA, even showing a visible aggregation effect. The aggregation was commonly believed as the formation of carbonyl compounds, dimeric tyrosine, disulfide bonds, or other oxidation products that cross-link and aggregate proteins.[59]

Figure 8 inset shows the photographic records of the process of BSA aggregation induced by the photolysis of H_2O_2 and the
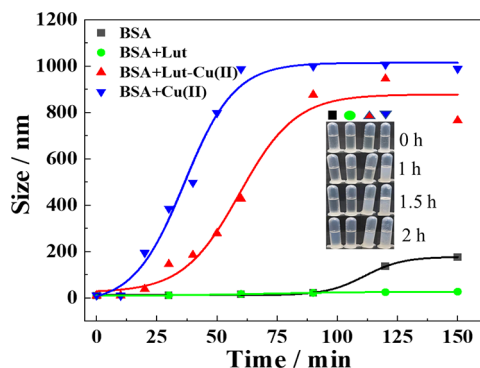

Figure 8. The kinetic changes in the size of BSA, BSA + Lut, BSA + Cu(II), and BSA + Cu(II)−Lut solution after both 254 and 365 nm UV irradiation in the MOPS buffer aqueous solution. Insets: photographed aggregation process of BSA, BSA + Lut, BSA + Cu(II), and BSA + Cu(II)−Lut, respectively. [BSA] = [Lut] = [Cu(II)] = 30 μM and [H_2O_2] = 4.9 M. The solid lines were obtained by Boltzmann model function fitting.

effects of the addition of Lut, Cu(II)−Lut, and Cu(II) to BSA. The sample with BSA alone started to turn turbid at 2 h, while the sample with BSA + Lut showed a clear inhibition of the aggregation of BSA and did not turn turbid within the time range of measurement. Coordination of Cu(II) to Lut showed clear turbidity at 1.5 h, significantly promoting the aggregation of BSA compared with the sample with Lut alone, but showed less effect than for Cu(II) alone, for which the turbidity increased earlier at 1 h.

The changes in the size of BSA during aggregation were also quantitatively recorded. It was evident that Lut, Cu(II)−Lut, and Cu(II) showed different effects on the oxidative aggregation of BSA as seen in Figure 8. The size of BSA alone increased very slowly to a minor extent up to 176 nm at 150 min. Lut showed a superior antioxidant effect such that the size for BSA with Lut did not change and was kept at ∼27 nm within 150 min, while both Cu(II)−Lut and Cu(II) showed significant pro-oxidation effects. The size of BSA with Cu(II)−Lut rapidly increased from ∼40 nm at 20 min to a constant ∼870 nm at 90 min, which resembled but had less effect than the sample with Cu(II) alone. The most remarkable aggregation up to ∼1000 nm at ∼60 min observed for BSA with Cu(II) alone was explained as the catalysis of dissociation of H_2O_2 into •OH by Cu(II) through a Fenton-like reaction similar to that seen in eqs 3 and 4 (R = H, ROOH = H_2O_2) to accelerate the oxidation of BSA and induce aggregation.

Polyphenol compounds were generally considered to be antioxidants in lipid oxidation but were also reported to show pro-oxidation behaviors on protein oxidation due to their auto-oxidation by O_2 to produce a reactive oxygen radical under some cases depending on concentrations.[60] The presence of transition metals or Fenton-reaction metal ions involved can further enhance the pro-oxidation activity of polyphenols by the promotion of self-oxidation.[60,61] However, a pro-oxidation effect was not seen in the present study for Lut, which showed inhibition activities in both carbonyl formation and protein aggregation. The Cu(II)−Lut complex showing a significant promotion effect in BSA aggregation supported that Cu(II) in the BSA−Cu(II)−Lut complex may still act as a catalyzer or pro-oxidant even if Cu(II) is chelated by the catechol group of Lut. Lut in the BSA−Cu(II)−Lut complex may still play an antioxidant role but with less effect than Lut alone, probably due to the coordination of Cu(II) blocking the active catechol group.

4. CONCLUSIONS

Cu(II) coordination promoted an additional Lut binding to BSA with a higher affinity and a more stabilized protein structure. Pro-oxidative Cu(II) coordinated to BSA was converted by Lut into an antioxidant through a shift in the coordination site and the formation of the Cu(II)−Lut complex in inhibiting the oxidation of free amino groups induced by the less reactive radical ROO•. However, for the system induced by a more reactive •OH radical, Cu(II) showed antagonistically a pro-oxidation effect on the antioxidation of Lut with BSA. This study may accordingly provide new perspectives for the further understanding of the

functions of flavonoids as important food components, additives, and antioxidants.

■ AUTHOR INFORMATION

Corresponding Author

Rui-Min Han − *Key Laboratory of Advanced Light Conversion Materials and Biophotonics, Department of Chemistry, Renmin University of China, Beijing 100872, China;* ● orcid.org/0000-0002-1293-8413; Phone: +86-10-6251-6604; Email: rmhan@ruc.edu.cn; Fax: +86-10-6251-6444

Authors

Meng-Ting Song − *Key Laboratory of Advanced Light Conversion Materials and Biophotonics, Department of Chemistry, Renmin University of China, Beijing 100872, China*

Wen-Zhu Wang − *Key Laboratory of Advanced Light Conversion Materials and Biophotonics, Department of Chemistry, Renmin University of China, Beijing 100872, China*

Yao Lu − *Key Laboratory of Advanced Light Conversion Materials and Biophotonics, Department of Chemistry, Renmin University of China, Beijing 100872, China*

Leif H. Skibsted − *Department of Food Science, University of Copenhagen, DK-1958 Frederiksberg C, Denmark;* ● orcid.org/0000-0003-1734-5016

Jian-Ping Zhang − *Key Laboratory of Advanced Light Conversion Materials and Biophotonics, Department of Chemistry, Renmin University of China, Beijing 100872, China;* ● orcid.org/0000-0002-9216-2386

Complete contact information is available at:
https://pubs.acs.org/10.1021/acsomega.2c01226

Notes

The authors declare no competing financial interest.

■ ABBREVIATIONS

SA serum albumin
BSA bovine serum albumin
HSA human serum albumin
Lut luteolin
ITC isothermal titration calorimetry
CD circular dichroism
AAPH 2,2′-azobis(2-methylpropionamidine) dihydrochloride
MOPS 3-(*N*-morpholino)propanesulfonic acid buffer solution
MD molecular dynamics
DNPH 2,4-dinitrophenylhydrazine
DTNB 3,3′-dithio-bis(6-nitrobenzoic acid)
RMSD root mean square deviation
Rg rotation radius
SASA solvent accessible surface area

■ REFERENCES

(1) He, X. M.; Carter, D. C. Atomic structure and chemistry of human serum albumin. *Nature* **1992**, *358*, 209−215.

(2) Huang, B. X.; Kim, H. Y.; Dass, C. Probing three-dimensional structure of bovine serum albumin by chemical cross-linking and mass spectrometry. *J. Am. Soc. Mass Spectrom.* **2004**, *15*, 1237−1247.

(3) Sengupta, P.; Sardar, P. S.; Roy, P.; Dasgupta, S.; Bose, A. Investigation on the interaction of Rutin with serum albumins: Insights from spectroscopic and molecular docking techniques. *J. Photochem. Photobiol. B.* **2018**, *183*, 101−110.

(4) Zhang, X.-F.; Xie, L.; Liu, Y.; Xiang, J.-F.; Tang, Y.-L. Binding of the bioactive component Aloe dihydroisocoumarin with human serum albumin. *J. Mol. Struct.* **2008**, *891*, 87−92.

(5) Ashbrook, J. D.; Spector, A. A.; Santos, E. C.; Fletcher, J. E. Long chain fatty acid binding to human plasma albumin. *J. Biol. Chem.* **1975**, *250*, 2333−2338.

(6) Zhao, Z.; Shi, T.; Chu, Y.; Cao, Y.; Chen, S.; Na, R.; Wang, Y. Comparison of the interactions of flupyrimin and nitenpyram with serum albumins via multiple analysis methods. *Chemosphere* **2022**, *289*, 133139−133148.

(7) Obrenovich, M. E.; Nair, N. G.; Beyaz, A.; Aliev, G.; Reddy, V. P. The role of polyphenolic antioxidants in health, disease, and aging. *Rejuvenation Res.* **2019**, *13*, 631−643.

(8) Pietta, P. G. Flavonoids as antioxidants. *J. Nat. Prod.* **2000**, *63*, 1035−1042.

(9) Yang, J.; Xu, Y.; Liu, H.-Y.; Han, R.-M.; Zhang, J.-P.; Skibsted, L. Genistein binding to copper(II)-solvent dependence and effects on radical scavenging. *Molecules* **2017**, *22*, 1757−1771.

(10) Xu, Y.; Qian, L.-L.; Yang, J.; Han, R.-M.; Zhang, J.-P.; Skibsted, L. H. Kaempferol binding to zinc(II), efficient radical scavenging through Increased phenol acidity. *J. Phys. Chem. B* **2018**, *122*, 10108−10117.

(11) Qian, L.-L.; Lu, Y.; Xu, Y.; Yang, Z.-Y.; Yang, J.; Zhou, Y.-M.; Han, R.-M.; Zhang, J.-P.; Skibsted, L. H. Alkaline earth metal ion coordination increases the radical scavenging efficiency of kaempferol. *RSC Adv.* **2020**, *10*, 30035−30047.

(12) Liu, C.; Wang, W.; Song, M.; Lu, Y.; Qian, L.; Han, R.; Zhang, J.; Skibsted, L. H. Radical scavenging efficiency of flavonoids increased by calcium(II) binding: structure-activity relationship. *ChemistrySelect* **2021**, *6*, 1−8470.

(13) Zhang, G.; Ma, Y.; Wang, L.; Zhang, Y.; Zhou, J. Multispectroscopic studies on the interaction of maltol, a food additive, with bovine serum albumin. *Food Chem.* **2012**, *133*, 264−270.

(14) Xiao, J.; Suzuki, M.; Jiang, X.; Chen, X.; Yamamoto, K.; Ren, F.; Xu, M. Influence of B-ring hydroxylation on interactions of flavonols with bovine serum albumin. *J. Agric. Food Chem.* **2008**, *56*, 2350−2356.

(15) Poloni, D. M.; Dangles, O.; Vinson, J. A. Binding of plant polyphenols to serum albumin and LDL: healthy implications for heart disease. *J. Agric. Food Chem.* **2019**, *67*, 9139−9147.

(16) Sarmah, S.; Das, S.; Roy, A. S. Protective actions of bioactive flavonoids chrysin and luteolin on the glyoxal induced formation of advanced glycation end products and aggregation of human serum albumin: In vitro and molecular docking analysis. *Int. J. Biol. Macromol.* **2020**, *165*, 2275−2285.

(17) Fu, L.; Sun, Y.; Ding, L.; Wang, Y.; Gao, Z.; Wu, Z.; Wang, S.; Li, W.; Bi, Y. Mechanism evaluation of the interactions between flavonoids and bovine serum albumin based on multi-spectroscopy, molecular docking and Q-TOF HR-MS analyses. *Food Chem.* **2016**, *203*, 150−157.

(18) Robinson, N. J.; Winge, D. R. Copper metallochaperones. *Annu. Rev. Biochem.* **2010**, *79*, 537−562.

(19) Bal, W.; Sokołowska, M.; Kurowska, E.; Faller, P. Binding of transition metal ions to albumin: sites, affinities and rates. *Biochim. Biophys. Acta* **2013**, *1830*, 5444−5455.

(20) Cao, S.; Jiang, X.; Chen, J. Effect of Zinc (II) on the interactions of bovine serum albumin with flavonols bearing different number of hydroxyl substituent on B-ring. *J. Inorg. Biochem.* **2010**, *104*, 146−152.

(21) Li, D.; Zhu, M.; Xu, C.; Chen, J.; Ji, B. The effect of Cu^{2+} or Fe^{3+} on the noncovalent binding of rutin with bovine serum albumin by spectroscopic analysis. *Spectrochim. Acta A.* **2011**, *78*, 74−79.

(22) Shi, S.; Zhang, Y.; Chen, X.; Peng, M. Investigation of flavonoids bearing different substituents on ring C and their Cu^{2+} complex binding with bovine serum albumin: structure-affinity relationship aspects. *J. Agric. Food Chem.* **2011**, *59*, 10761−10769.

(23) Gökmen, A.; Kúsz, N.; Karaca, N.; Demirci, F.; Hohmann, J.; Kirmizibekmez, H. Secondary metabolites from verbascum bugulifolium Lam. and their bioactivities. *Nat. Prod. Res.* **2021**, *35*, 5294−5298.

(24) Xu, Y.; Yang, J.; Lu, Y.; Qian, L.; Yang, Z.; Han, R.; Zhang, J.; Skibsted, L. H. Copper(II) coordination and translocation in luteolin and effect on radical scavenging. *J. Phys. Chem. B* **2020**, *124*, 380−388.

(25) Bi, S.; Yan, L.; Wang, Y.; Pang, B.; Wang, T. Spectroscopic study on the interaction of eugenol with salmon sperm DNA in vitro. *J. Lumin.* **2012**, *132*, 2355−2360.

(26) Keswani, N.; Kishore, N. Calorimetric and spectroscopic studies on the interaction of anticancer drug mitoxantrone with human serum albumin. *J. Chem. Thermodyn.* **2011**, *43*, 1406−1413.

(27) Krieger, E.; Dunbrack, R. L., Jr.; Hooft, R. W. W.; Krieger, B. Assignment of protonation states in proteins and ligands: combining pKa prediction with hydrogen bonding network optimization. *Methods Mol. Biol.* **2012**, *819*, 405−421.

(28) Maier, J. A.; Martinez, C.; Kasavajhala, K.; Wickstrom, L.; Hauser, K. E.; Simmerling, C. ff14SB: improving the accuracy of protein side chain and backbone parameters from ff99SB. *J. Chem. Theory Comput.* **2015**, *11*, 3696−3713.

(29) Wang, J.; Wolf, R. M.; Caldwell, J. W.; Kollman, P. A.; Case, D. A. Development and testing of a general amber force field. *J. Comput. Chem.* **2004**, *25*, 1157−1174.

(30) Jakalian, A.; Jack, D. B.; Bayly, C. I. Fast, efficient generation of high-quality atomic charges. AM1-BCC model: II. Parameterization and validation. *J. Comput. Chem.* **2002**, *23*, 1623−1641.

(31) Essman, U.; Perera, L.; Berkowitz, M. L.; Darden, T.; Lee, H.; Pedersen, L. G. A smooth particle mesh Ewald method. *J. Chem. Phys.* **1995**, *103*, 8577−8593.

(32) Lin, C.; Hu, M.; Wu, A.; Zhu, C. Investigation on the differences of four flavonoids with similar structure binding to Human serum albumin. *J. Pharm. Biomed.* **2014**, *4*, 392−398.

(33) Dolidze, T.; Makharadze, M.; Uchaneishvili, S.; Nioradze, N.; Laliashvili, L. New aspects of the interaction of copper(II) with serum albumin: voltammerric and microcalorimetric studies. *Georgian Med. News.* **2021**, *318*, 139−142.

(34) Stewart, J. J. P. Optimization of parameters for semiempirical methods. III. Extension of PM3 to Be, Mg, Zn, Ga, Ge, As, Se, Cd, In, Sn, Sb, Te, Hg, Tl, Pb, and Bi. *J. Comput. Chem.* **1991**, *12*, 320−341.

(35) Stewart, J. J. P. MOPAC: a semiempirical molecular orbital program. *J. Comput. Aid. Mol. Des.* **1990**, *4*, 1−103.

(36) Sanner, M. F. Python: a programming language for software integration and development. *J. Mol. Graphics Modell.* **1999**, *17*, 57−61.

(37) Precupas, A.; Sandu, R.; Leonties, A. R.; Anghel, D.-F.; Popa, V. T. Complex interaction of caffeic acid with bovine serum albumin: calorimetric, spectroscopic and molecular docking evidence. *New J. Chem.* **2017**, *41*, 15003−15015.

(38) Levine, R. L.; Williams, J. A.; Stadtman, E. R.; Schacter, E. Carbonyl assays for determination of oxidatively modified proteins. *Methods Enzymol.* **1994**, *233*, 346−357.

(39) Baron, C. P.; Refsgaard, H. H. F.; Skibsted, L. H.; Andersen, M. L. Oxidation of bovine serum albumin initiated by the Fenton reaction-effect of EDTA, tert-butylhydroperoxide and tetrahydrofuran. *Free Radical Res.* **2006**, *40*, 409−417.

(40) Davies, K. J.; Delsignore, M. E.; Lin, S. W. Protein damage and degradation by oxygen radicals. II. Modification of amino acids. *J. Biol. Chem.* **1987**, *262*, 9902−9907.

(41) Di Simplicio, P.; Chesseman, K. H.; Slater, T. F. The reactivity of the sh group of bovine serum albumin with free radicals. *Free Radical Res.* **1991**, *14*, 253−262.

(42) Chen, Z.; Leinisch, F.; Greco, I.; Zhang, W.; Shu, N.; Chuang, C. Y.; Lund, M. N.; Davies, M. J. Characterisation and quantification of protein oxidative modifications and amino acid racemisation in powdered infant milk formula. *Free Radical Res.* **2019**, *53*, 68−81.

(43) Naso, L. G.; Lezama, L.; Valcarcel, M.; Salado, C.; Villacé, P.; Kortazar, D.; Ferrer, E. G.; Williams, P. A. Bovine serum albumin binding, antioxidant and anticancer properties of an oxidovanadium-(IV) complex with luteolin. *J. Inorg. Biochem.* **2016**, *157*, 80−93.

(44) Qi, Z.; Zhang, Y.; Liao, F.; Ou-Yang, Y.; Liu, Y.; Yang, X. Probing the binding of morin to human serum albumin by optical spectroscopy. *J. Pharm. Biomed. Anal.* **2008**, *46*, 699−706.

(45) Malacaria, L.; La Torre, C.; Furia, E.; Fazio, A.; Caroleo, M. C.; Cione, E.; Gallelli, L.; Marino, T.; Plastina, P. J. Aluminum(III), iron(III) and copper(II) complexes of luteolin: Stability, antioxidant, and anti-inflammatory properties. *Mol. Liq.* **2022**, *345*, 117895−117906.

(46) Říha, M.; Karlíčková, J.; Filipský, T.; Macáková, K.; Rocha, L.; Bovicelli, P.; Silvestri, I. P.; Saso, L.; Jahodář, L.; Hrdina, R.; Mladěnka, P. In vitro evaluation of copper-chelating properties of flavonoids. *RSC Adv.* **2014**, *4*, 32628−32638.

(47) Papadopoulou, A.; Green, R. J.; Frazier, R. A. Interaction of flavonoids with bovine serum albumin: a fluorescence quenching study. *J. Agric. Food Chem.* **2005**, *53*, 158−163.

(48) Soares, S.; Mateus, N.; Freitas, V. Interaction of different polyphenols with bovine serum albumin (BSA) and human salivary α-amylase (HSA) by fluorescence quenching. *J. Agric. Food Chem.* **2007**, *55*, 6726−6735.

(49) Sengupta, P.; Pal, U.; Mondal, P.; Bose, A. Multi-spectroscopic and computational evaluation on the binding of sinapic acid and its Cu(II) complex with bovine serum albumin. *Food Chem.* **2019**, *301*, 125254−125264.

(50) Zhang, L.; Zhao, X.; Tao, G.-J.; Chen, J.; Zheng, Z.-P. Investigating the inhibitory activity and mechanism differences between norartocarpetin and luteolin for tyrosinase: A combinatory kinetic study and computational simulation analysis. *Food Chem.* **2017**, *223*, 40−48.

(51) Wang, Y.-Q.; Zhang, H.-M. Comparative studies of the binding of six phthalate plasticizers to pepsin by multispectroscopic approach and molecular modeling. *J. Agric. Food Chem.* **2013**, *61*, 11191−11200.

(52) Sengupta, P.; Pal, U.; Roy, P.; Samanta, T.; Chattopadhyay, N.; Sen, K.; Bose, A. Effect of a metal Ion in modulating the binding interaction of a dietary flavonoid with bovine serum albumin and DNA: a spectroscopic and theoretical approach. *ACS Food Sci. Technol.* **2022**, *2*, 114−124.

(53) Sudlow, G.; Birkett, D. J.; Wade, D. N. Further characterization of specific drug binding sites on human serum albumin. *Mol. Pharmacol.* **1976**, *12*, 1052−1061.

(54) Yang, Y.; Hu, Q.; Fan, Y.; Shen, H. Study on the binding of luteolin to bovine serum albumin. *Spectrochim. Acta A.* **2008**, *69*, 432−436.

(55) Charbonneau, D.; Beauregard, M.; Tajmir-Riahi, H. A. Structural analysis of human serum albumin complexes with cationic lipids. *J. Phys. Chem. B* **2009**, *113*, 1777−1784.

(56) Kou, Y.; Lu, J.; Jiang, X.; Tian, B.; Xue, Y.; Wang, M.; Tan, L. Electrochemical determination of vitamin B12 based on Cu^{2+}-involved fenton-like reaction. *Electroanalysis* **2019**, *31*, 1−10.

(57) Dahiya, A.; Patel, B. K. The rich legacy and bright future of transition-metal catalyzed peroxide based radical reactions. *Chem. Rec.* **2021**, *21*, 3589−3612.

(58) Ignasiak, M.; Frackowiak, K.; Pedzinski, T.; Davies, M. J.; Marciniak, B. Unexpected light emission from tyrosyl radicals as a probe for tyrosine oxidation. *Free Radical Biol. Med.* **2020**, *153*, 12−16.

(59) Cui, X.; Xiong, Y. L.; Kong, B.; Zhao, X.; Liu, N. Hydroxyl radical-stressed whey protein isolate: chemical and structural properties. *Food Bioproc. Tech.* **2012**, *5*, 2454−2461.

(60) Utrera, M.; Estévez, M. Analysis of tryptophan oxidation by fluorescence spectroscopy: effect of metal-catalyzed oxidation and selected phenolic compounds. *Food Chem.* **2012**, *135*, 88−93.

(61) Procházková, D.; Boušová, I.; Wilhelmová, N. Antioxidant and prooxidant properties of flavonoids. *Fitoterapia* **2011**, *82*, 513−523.